



Project 103 Pareto Efficient SAF Yield and Blending

Washington State University

Project Lead Investigator

Joshua Heyne
Bioproducts, Sciences, and Engineering Laboratory Director, Associate Professor
School of Engineering and Applied Science
2710 Crimson Way, Richland, WA 99354
(937) 229-5319
joshua.heyne@wsu.edu

University Participants

Washington State University

- P.I.: Dr. Joshua Heyne
- FAA Award Number: 13-C-AJFE-WaSU-044
- Period of Performance: October 01, 2024, to September 30, 2025
- Tasks:
 1. Distillation optimization tool and procedure improvement
 2. Vapor pressure measurement for sustainable aviation fuel (SAF)

Project Funding Level

The Federal Aviation Administration (FAA) provided \$350,000 in funding; cost sharing is provided by Air Company (\$200,000) and Trinity College Dublin (\$150,000).

Investigation Team

Washington State University

Joshua Heyne (P.I.), Coordinating all team members (both ASCENT and non-ASCENT efforts) and communicating distillation results with SAF producers.
Randall Boehm, Research Engineer, Overseeing the project and providing guidance.
Zhibin (Harrison) Yang, Research Engineer, Conducting distillation optimization and property measurements.
Alexander Kelly (Ph.D. student), Conducting distillation and modeling.

Project Overview

The ASCENT Project 103 supports the conversion of pilot-scale bio-crude samples into plausible aviation fuel blend components, up to 100%, with the balance coming from a petroleum distillate. For non-selective sustainable aviation fuels production processes, the product stream could contain species ranging from as few as five to many (>26) carbon atoms per molecule (distillation range, 36°C to greater than 450°C), which is broader than the jet fuel range. In these cases, distillation can be used to separate the product stream into fractions, where the monetary value of each fraction varies based on contemporary policies, and the properties of that fraction. While this is essentially the same process as petroleum refining, the population distribution of different molecular species within a given distillation cut could be markedly different depending on the pathway, and composition differences result in significant property differences.



Task 1 – Distillation Optimization Tool and Procedure Improvement

Washington State University

Objectives

The objectives of this task are intended to improve the current distillation optimization tool, Jet Fuel Blend Optimizer (JudO), and procedures associated with distillation processes to improve yield for a given SAF candidate while keeping the properties within the specification limits.

Research Approach

Introduction

Volatility properties of jet fuels are known to have some impact on the safe operation of aircraft. As such, certain representative properties are specified in governing specifications such as ASTM D1655 (ASTM International, 2023), DEF STAN 91-091 (Ministry of Defence, 2025), and GB/T 6539-1997 (State Bureau of Technical Supervision, 1997). The flash point relates to aircraft-level fire safety. The initial boiling point relates to fuel pump cavitation and fuel control instabilities that could be caused by two-phase flow. The temperature at which 10% of petroleum-derived jet fuel (T10) has vaporized is correlated with engine ignition characteristics. During thermal soak-back after a jet engine is shut off, the vapor pressure inside the closed circuit from the fuel metering unit to the fuel nozzle valves could exceed the valve cracking pressure and lead to fuel burping into the fuel nozzles where it can bake until it turns to coke. A similar phenomenon can happen during part-power operation, when some fuel circuits are turned off (called staging). The dry-out rate of passively purged, staged fuel circuits, similar to droplet evaporation rates, depends on the mass transfer rate, vapor pressure and liquid-phase surface area. Finally, the end point of the distillation is correlated with combustor coking and unburned hydrocarbon emissions. None of these relationships are one-to-one. Moreover, the above listing of operating concerns that could potentially be impacted by fuel properties is not exhaustive. Indeed, an exhaustive list of potential concerns is not generally known (Colket & Heyne, 2021). Motivated by such known and unknown factors, two volatility properties, (T50-T10) and (T90-T10), where the subscript refers to the volume fraction distilled, were added as “extended requirements” in the quality specification, ASTM D7566 (ASTM International, 2022a), governing aviation turbine fuels containing synthesized hydrocarbons.

Specifically, the rate of evaporation across a plurality of temperature, convective, and dwell time conditions is directly related to potential operating concerns. Unlike measure temperature (T_n), the vapor pressure (P_{vap}) of fuel droplets or sheets is directly proportional to their evaporation rate under all operating conditions. The importance of this is recognized by the community, and as such, the vapor pressure as a function of temperature is listed as a Tier 2 property in ASTM D4054 (ASTM International, 2023). While maintaining an approximate match to a family of P_{vap} versus temperature curves derived from a representative survey of petroleum-derived jet fuels is a prudent goal for developers of SAF or other fuels with synthetic components, it is neither sufficient nor necessary in all circumstances.

SAF and synthetic blending components (SBC) are considered mid-term solutions to help decarbonize the aviation sector by 2050 (IATA, 2025). The term SAF is primarily used in policy and regulatory contexts, whereas SBC is the corresponding technical term used in fuel qualification standards. Currently, SBCs are limited up to 50% by volume when blended with conventional jet fuel, because some pathways (e.g., hydroprocessed esters and fatty acids synthetic paraffinic kerosene) lack certain hydrocarbon classes such as aromatics, which are necessary for elastomer swelling and ensuring proper fuel system performance. To overcome this limitation and enable 100% synthetic ‘drop-in’ jet fuels, the aviation community is exploring blending multiple ASTM D7566 annexes. However, original equipment manufacturers (OEM), prioritizing safety and reliability, have emphasized the need to evaluate ASTM D4054 Tier 2 or fit-for-purpose (FFP) properties to ensure that fully synthetic fuels meet operational requirements. Measuring all FFP properties experimentally is costly and often beyond the capabilities of many refineries. As a result, the ability to accurately predict FFP properties, particularly volatility and vapor pressure, has become a high priority within the fuel community, as it would accelerate certification, enable higher SAF blend limits, and ultimately support aviation decarbonization efforts.

The chemical (and, to a lesser extent, transport) properties of fuel vapor vary throughout the evaporation time scale, and so do the volatility properties of the liquid that have yet to evaporate. Chemical properties (represented by the derived cetane number, radical index, threshold sooting index, etc.) play an important role in lean blowout, non-volatile particulate matter (nvPM) emissions and the rate of heat release during combustion, indicating a potential impact on combustion dynamics, combustor temperature distribution and combustion efficiency, for example. The composition of the remaining liquid, in tandem with the temperature at its interface with air, determines its vapor pressure and hence its evaporation



rate for the relevant transport conditions. All these variances are hereafter referred to as preferential evaporation in this article.

Property models that neglect to track changes in liquid-phase composition throughout the evaporation time scale sacrifice the capability to directly capture the impact of preferential evaporation. However, through correlation with specific points on the ASTM D86 (ASTM International, 2024a) distillation curve, some indirect capturing of preferential evaporation may occur, provided that the relative population distribution of each type of hydrocarbon in the boiling sample is similar to the database of fuel samples from which the model was built. Mendes et al. (2017) published a regression model to predict the Reid vapor pressure (P_{vap} at 37.8°C) of conventional gasoline based on its ASTM D86 distillation curve. Two groups (Cooper et al., 1995; Flecher et al., 1997) published separate regression models built from Raman spectrographic data to predict Reid vapor pressure and octane numbers of petroleum fuels. Flumignan et al. (2008) built a regression model built from chromatographic data to predict the density, distillation curve and octane numbers of Brazilian gasoline, while Cocco et al. (2005) used chromatographic data of 25 samples to build an artificial neural network model to predict the density, distillation curve and Reid vapor pressure of Brazilian gasoline. It is unknown whether any of these models capture the impact of preferential evaporation, even for petroleum-derived gasoline, or whether any are valid for jet fuel range hydrocarbons.

Other notable examples of simulated ASTM D86 distillation curves include ASTM D2887 (ASTM International, 2024b) (which employs chromatographic data) and the work of Mondragon and Ouchi (1984) (which employs thermogravimetric data). The intense interest around this task is a testimonial to its value, which appears to be rooted in the reduction in sample volume required to determine properties that are controlled by some quality specification. Not only do such models neglect to directly capture the impact of preferential vaporization, but they offer little value to efforts, such as those described by Miller et al. (2022), to maximize biomass in SAF by optimal selection of distillation fractions or other refinement processes of the synthetic blend component. Furthermore, such models, barring a simulation of the base data, do still necessitate some mass of representative sample to obtain the input data.

Within the so-called tier- α suite of property models published by Yang et al. (2021), vapor pressure is calculated by Dalton's Law, with partial pressures calculated by Raoult's Law, and simulated D86 distillation is carried out by incremental mass extraction per the composition of the simulated vapor phase. Miller et al. (2022) now execute simulated distillation using this same approach and have observed significant error in the prediction of T90. Such error could stem from distillation assumptions (e.g., the number of theoretical plates), inaccurate composition input or propagated errors in components' vapor pressures.

In a provocative article published in 1995, Hawkes (1995) proclaimed that Raoult's Law is deceptive, which is somewhat interesting in that Wilson's model of activity coefficients was introduced in 1964 (Wilson, 1964), and it was already common by then, in some circles, to use activity coefficients to scale the partial pressures that are predicted by Raoult's Law to arrive at a more accurate description of the vapor-liquid-phase equilibrium. By 1975, the unsettling fact that vapor-liquid equilibrium data were needed to determine one or more of the parameters used in the Wilson model (and several of its off-shoots) was addressed by Fredenslund et al. (1975) by relating these terms to groups (e.g., >C<, -CH₃, aromatic CH, etc.) that are contained in all molecules where the contributions from each group were determined by fitting to vapor-liquid equilibrium data for a variety of binary mixtures, which in theory would permanently establish these contributions so they could be used without modification for other molecules and mixtures that were not part of the original database. This model is called the UNIFAC (UNIQUAC Functional-group Activity Coefficients) model and is included in publicly available software such as Aspen Plus, DWSIM, and ChemCAD. It is simple enough to be implemented within a spreadsheet such as Microsoft® Excel®, which is what we did to enable comparisons with the new model presented in this work. This spreadsheet is included in the Supplementary Materials, entitled, "UNIFAC Vapor Pressures." Yet more fundamental models based on intermolecular potentials (RGEMC) (Lisal et al., 1999) or simulated osmotic pressure (OMD) (Crozier & Rowley, 2002) are available in molecular dynamics software such as LAMMPS, while Reference Fluid Thermodynamic and Transport Properties Database (REFPROP) (Lemmon et al., 2013) employs mixing rules to develop an equation of state for the mixture (Kunz & Wagner, 2012) from which many properties can be calculated, including vapor pressure.

Here, our goal is to evaluate simpler corrections to Raoult's Law as fuels comprise thousands of different molecules, and simulated fuel distillations may require several thousand determinations of the vapor-liquid equilibrium. Among these thousands of molecules, only seven carbon types are significantly represented; four aliphatic carbon types (-CH₃, -CH₂-,

® Microsoft and Excel are registered trademarks of Microsoft Corporation in the United States and other countries.



>CH- and >C<) and three aromatic carbon types (protonated aromatic carbon, substituted aromatic carbon and bridgehead aromatic carbon). Within UNIFAC, four terms are used to represent the four aliphatic carbon types, and two terms are used to represent aromatic carbon, protonated or not protonated. In contrast, we are not distinguishing between carbon types or molecular structure. Rather, we acknowledge that every molecule is forced into an environment determined by the liquid mixture's Gibbs energy minima, which differs significantly from that of pure liquids and is the root cause of a non-zero heat of mixing. While the magnitude of the heat of mixing is approximately 500 times less than the magnitude of the heat of vaporization, we postulate that enthalpy difference can have a significant impact on the vapor pressure of each liquid mixture component. The main effect on the heat of mixing of jet fuel-range hydrocarbons is the mole fraction, not molecular structure, so here we develop a model framework that is based exclusively on mole fractions as input and a tuning database of binary mixture vapor pressures where the (much) more volatile component is present at mole fractions ranging from 0.01 to 0.09. Over this range of mole fractions, the traditional activity coefficient approach to correcting Raoult's Law is not validated to the best of the authors' knowledge.

The approach we considered is described below. Then, we describe the materials, test conditions and testing methodology used to support determination of the adjustable parameters of this modeling approach, and the derivation of empirically based correction. Validation of the resulting model is accomplished by comparing modeled vapor-liquid equilibrium systems with experimental measurements. Finally, a summary of the major findings of this study is presented in the "Results" and "Conclusions" sections.

Theory

Background

The earliest model of vapor pressure can be traced back to Clapeyron (1834), nearly 190 years ago. Since then, many model refinements have been published, starting with Clausius (1850), who published the form that is found in many current physical or general chemistry textbooks. These models relate the vapor pressure of a liquid to its latent heat of vaporization (ΔH_{vap}) and imply that $(\Delta H_{vap}/R)$ equals the slope of $\ln(P_{vap})$ versus inverse temperature ($1/T$). Interestingly, the general form of this model can also be derived from kinetic theory, although it was originally conceived entirely from fundamental principles of thermodynamics. Trouton (1884) shared a recognition that the entropy of vaporization at the ambient pressure of most liquids is approximately the same, $87.3 \text{ J}\cdot\text{K}^{-1}\cdot\text{mol}^{-1}$, which implies that ΔH_{vap} is directly proportional to the normal boiling point.

By definition, the vapor pressure of a substance is the pressure at which the rate of adsorption of gaseous molecules that strike the surface of a liquid equals the rate of desorption of molecules from the surface of that liquid. The evaporation rate is the difference between the rate of desorption and the rate of adsorption and goes to zero at equilibrium. Theoretically, the rate of desorption of any component in a liquid mixture could be limited by the diffusion of volatile molecules to the surface or by the fundamental process of desorption.

As accommodated by Antoine (1888) semiempirical correction to the vapor pressure model, the activation energies of whatever steps control the rate of desorption in pure materials are not generally equal to ΔH_{vap} as, by definition, ΔH_{vap} is the enthalpy difference between the liquid and gaseous phases of the material. The activation energy is coincidentally nearly equal to ΔH_{vap} in many systems. However, the desorption process could occur in multiple steps, and the activation energy governing the rate of each step is, more likely than not, greater than the energy difference between the two geometrical configurations that define the step. In other words, even for pure materials, the slope of $\ln(P_{vap})$ versus inverse temperature ($1/T$) could be higher or lower than ΔH_{vap} .

As recognized by Antoine (1888) and many authors since then Poling et al. (2001), $\ln(P_{vap})$ is not exactly linear with ($1/T$), which suggests that the rate limiting steps in the desorption process are influenced by the bulk change in molar volume as temperature varies. In other words, it matters how many first or second nearest neighbors to a desorbing molecule are vacant. By extension, it should also matter how many first or second nearest neighbors are heterogeneous molecules. To estimate the order of magnitude of this effect, we compare the heat of mixing, which is approximately 25 J/mol (Lundberg, 1964) for jet fuel-range hydrocarbons, to the heat of vaporization of a representative fuel molecule, n-dodecane, which is 44,000 J/mol. While the heat of mixing has a small (<0.1%) impact on the heat of vaporization, its impact on the desorption rate is approximately 0.6% at the normal boiling temperature of n-dodecane. Intuitively, this impact increases as the mole fraction decreases because molecules of this mixture component are progressively less likely to have homogeneous neighbors as the mole fraction decreases.



For a more fundamental description of the relationship between the molecular arrangements in the condensed phase and the mobility of molecules or vacancies within the condensed phase, the reader is referred to Gaudin and Ma (2020). Briefly, in the condensed phase (the liquid), the desorbing molecule from a mixture sometimes originates (departs) from a shallower (potential energy surface) well than it would if it were not mixed with heterogeneous molecules, but essentially never originates from a deeper well. This is because optimal molecular packing in the condensed phase occurs when all the molecules are the same size and solutes are essentially forced into a packing arrangement that is determined by the solvent. The corresponding transition state, however, is less impacted by the mixture-induced geometric distortions of the condensed-phase lattice. This results in a lower effective activation energy. Quantifying this energy difference from first principles would be very difficult. Instead, we simply acknowledge that it should be lower and dependent on the mole fraction and use measured vapor pressures to gauge its magnitude.

Raoult's Law, in combination with a somewhat modified version of the Clausius–Clapeyron equation, is reproduced here as Equation 1, where x_i is the mole fraction, P_{ref} is 1 atm, $T_{ref,i}$ is the normal boiling point of pure component i and the remaining term is expanded below. The activation energy ($E_{a,i}$) varies with temperature and the actual vapor pressure of pure component i according to Equation 2, such that Equation 1 returns a correct vapor pressure at all temperatures, within the range of the data, when the mole fraction is unity. Pragmatically, an Antoine equation or a Wagner (1973) equation is used to represent discrete ($T, P_{vap,i}$) data points continuously, for each pure component. A spline is used to represent $E_{a,i}$ over the range of temperature $\pm 5^\circ\text{C}$ from the normal boiling point.

$$P_{vap,i} = x_i * P_{ref} * \exp \left[\left(\frac{E_{a,i}}{T_{ref,i}} \right) * \left(1 - \left(\frac{T_{ref,i}}{T} \right) \right) \right] \quad (\text{Eq. 1})$$

$$E_{a,i} = \ln \left(\frac{P_{vap,i}}{P_{ref}} \right) / \left[\left(1 / T_{ref,i} \right) - \left(1 / T \right) \right] \quad (\text{Eq. 2})$$

The reason why Equation 1 fails to accurately represent the actual partial pressure of component i in the vapor phase ($P_{vap,i}$) is not just because $E_{a,i}$ varies as the identity of nearest neighbors changes but also because the reference temperature ($T_{ref,i}$, the temperature at which $P_{vap,i} = x_i * 1 \text{ atm}$) varies as the effective surface area of the i th component, its concentration, varies. The desorption rate scales with the mole fraction (surface coverage) while the adsorption rate does not. In other words, both ($E_{a,i}$) and ($T_{ref,i}$) are concentration-dependent but the conventional approach to remediate the failure of Raoult's Law is to maintain each of these terms as constant and instead scale the resulting partial pressure by an activity coefficient, which depends not only on the identity of the i th component but also on its concentration, the temperature of the system and the identity and concentration of every other component in the mixture. Here, we evaluate simpler ways to make this correction.

Data Reduction Strategy

We consider replacing ($E_{a,i}$) and/or either or both occurrences of ($T_{ref,i}$) in Equation 1 with a simple, parameterized function of the mole fraction, the exact form of which is to be determined, for the purpose of minimizing the root mean square error (RMSE) of the predicted vapor pressure relative to the measured vapor pressure. These variants of Equation 1 are expressed here as Equations 3a through 3d. Ultimately, one (or none) of these equations will be recommended for the vapor pressure, evaporation rate and distillation simulation of complex fuels. For comparison, the activity coefficient approach is represented by the UNIFAC model.

$$P_{vap,i} = x_i * P_{ref} * \exp \left[\left(\frac{E_{a,i}}{T_{ref,i}} \right) * \left(1 - \left(\frac{A(x_i)}{T} \right) \right) \right] \quad (\text{Eq. 3a})$$

$$P_{vap,i} = x_i * P_{ref} * \exp \left[\left(\frac{B(x_i)}{T_{ref,i}} \right) * \left(1 - \left(\frac{T_{ref,i}}{T} \right) \right) \right] \quad (\text{Eq. 3b})$$

$$P_{vap,i} = x_i * P_{ref} * \exp \left[\left(\frac{E_{a,i}}{C(x_i)} \right) * \left(1 - \left(\frac{C(x_i)}{T} \right) \right) \right] \quad (\text{Eq. 3c})$$

$$P_{vap,i} = x_i * P_{ref} * \exp \left[\left(\frac{B(x_i)}{C(x_i)} \right) * \left(1 - \left(\frac{C(x_i)}{T} \right) \right) \right] \quad (\text{Eq. 3d})$$

In these equations, $A(x_i)$ and $C(x_i)$ are scaled reference temperatures, while $B(x_i)$ is a scaled activation energy. Two functional forms of the scale factor were tried for each term, where s is adjusted to minimize the RMSE. The trial 1 scale factor provided a lower RMSE in every case.



$$\text{Trial 1 scaling: } A(x), C(x) = T_{ref}^0 * (1 + s - s * x_i) \text{ or } B(x) = E_a^0 * (1 + s - s * x_i) \quad (\text{Eq. 4a})$$

$$\text{Trial 2 scaling: } A(x), C(x) = T_{ref}^0 * (1 - s/1.001 + s/(x_i + 0.001)) \text{ or } B(x) = E_a^0 * (1 - s/1.001 + s/(x_i + 0.001)) \quad (\text{Eq. 4b})$$

The same value of s applies to all three components, n-pentane, toluene and n-dodecane, as well as (conceptually) every component in jet fuel. A different value of s was determined for each model ([3a] through [3d]). For model (3d), two separate tuning parameters were derived, (1) for $B(x_i)$ and (2) for $C(x_i)$, and not surprisingly, this model provided the lowest RMSE of the set. Relative to the UNIFAC modeling scheme, this modeling approach sacrifices dependencies on component identity (differences in interaction energies, molecular shape and size) in favor of simplicity and generality. It also potentially gains an ability to elegantly capture some of the composition-specific temperature dependencies through its linkage to the Clausius–Clapeyron equation and the best available, temperature-dependent component data.

Reference Model (UNIFAC) Description

The UNIFAC model is described in detail by Fredenslund et al. (1975) and is one of several derivatives of earlier models of activity coefficients. In this model, the activity coefficient of component i is assumed to be a product of two terms: (1) the combinatorial term and (2) the residual term.

The log of the combinatorial term is then estimated by the sum of four more terms, involving six different terms, one of which is the mole fraction of component i , and another of which is a modeling constant set equal to 10. The four remaining terms are different arithmetic combinations of mole fractions, van der Waals volumes, and van der Waals surface areas of every component in the mixture.

The log of the residual term is the sum, over all groups (-CH₃, etc.) in the mixture, of the difference between two new terms, where one of these relates to the group's contribution in the mixture and the other relates to the group's contribution in pure component i . The same expression is used to define each of the 'new' terms. The independent parameters in this expression include the van der Waals surface area of each group, as well as the group fraction (analogous to the mole fraction), and it involves a group interaction parameter. A large set of group interaction parameters was determined by Fredenslund et al. (1975) through a non-linear, least squares data reduction scheme, where vapor-liquid (and liquid-liquid) equilibrium data of binary systems from 200 different sources were used as the foundational database.

The molecules used in this work comprise four groups: -CH₃, -CH₂-, arCH and arC-CH₃. The methyl group of toluene is combined with the aromatic carbon that it is bound to, and this pair is treated as one group. All four of these groups contribute uniquely to the van der Waals volume and surface area calculations, but for the purpose of interaction parameters, the methyl and ethyl groups are considered identical. However, the interaction terms (a) are not symmetric so $a_{mn} \neq a_{nm}$, meaning that we have to consider six interaction terms rather than three. A compilation of the values used in this work is provided in Table 1. The spreadsheet used to compile all of the arithmetic combinations of these parameters is provided in the Supplementary Material, entitled "UNIFAC Vapor Pressures."

Table 1. Fundamental UNIFAC parameters used in this work.

Molecular Group	vdW Volume	vdW Surface Area	a_{12}	a_{21}
-CH ₃	0.9011	0.848	-	-
-CH ₂ -	0.6744	0.540	-	-
arCH	0.5313	0.400	-	-
arC-CH ₃	1.2663	0.968	-	-
CH ₂ :: arCH	-	-	32.08	15.26
CH ₂ :: arC-CH ₃	-	-	26.78	-15.84
arCH :: arC-CH ₃	-	-	167.0	-146.8



Comparative Summary of Pressure Models

A number of different models applicable to pressure have already been mentioned in this manuscript (summarized in Table 2), and these are merely representative of a much larger population of models that we segregate into three intersecting purposes. Vapor pressure models of pure compounds (i.e., Clausius–Clapeyron, Antoine, Wagner) describe the relationship between the temperature of the system and its vapor pressure, where the gas and liquid phases are in equilibrium. The algebraically simplest of these, the Clausius–Clapeyron equation, is derived from fundamental theory and contains no empirically tuned parameters to correct for assumptions made in its derivation. The Antoine and Wagner equations leverage the fundamental relationship that vapor pressure is exponentially related to the inverse of temperature but use empirically tuned parameters to extend the applicable temperature and pressure range of the model, where the Wagner model extends applicability well into the supercritical region, beyond the critical temperature (T_{cr}) and critical pressure (P_{cr}). The Antoine and Wagner equations, via their reliance on measured pressures and temperatures, necessarily account for real gas deviation from ideal gas behavior. The simplest of all equations of state is the ideal gas law, but it applies only to gases with weak intermolecular force fields with a mean free path much larger than the molecular diameter. Several other equations of state similarly apply only to gases but with allowance, through empirically tuned parameters, for intermolecular attractions/repulsions and molecular volume. Some of the more sophisticated equations of state can also be used for characterizing the boundary (in pressure, temperature coordinates) between the gas and liquid phases, which is an alternative way of saying, “the vapor pressure curve.” Most of these models were developed for pure materials but can be extended to mixtures. For example, Opacich et al. (2019) used measured data to fit an Antoine equation for each jet fuel within scope in order to characterize its vapor pressure across a broad temperature range. Rauch (2017) made a systematic accuracy assessment for alternative aviation fuel evaporation models, which included an examination of fuel surrogates and simple vapor pressure models. In another approach, blending rules can be applied to the tuning parameters used in equations of state, with the complication that heterogeneous intermolecular interaction terms require measured data to determine their values. In both of these examples, the necessity for some measured data to build (or refine) the model severely restricts their scope of applicability.

For Raoult’s Law, the model captures the two main effects that contribute to the vapor pressure of a liquid mixture; namely the set of liquid-phase mole fractions and the set of the vapor pressures of each corresponding liquid component, but it is not as accurate as required for many applications. Among the early attempts to improve Raoult’s Law, Wilson (1964) introduced a scaling term (activity coefficient) that ultimately required some measured data pertaining to the mixture of scope to empirically derive parameters used in their model and predict activity coefficients. This approach, whether or not it yielded a more robust model than a mixture-specific Antoine (or Wagner) equation, suffers from a similar restriction on its scope of applicability for the same reason; measured data pertaining to the liquid of scope are required to finish constructing the model. The UNIFAC model eliminated the need for mixture-specific measurements to finish the model. However, its accuracy is not great, and it is more complex than desired for some applications. This work combines Raoult’s Law with a generalized form of the Clausius–Clapeyron equation, yielding a simple algebraic equation that depends on two tuned parameters that are applicable to all aliphatic and aromatic hydrocarbons, the set of liquid-phase mole fractions, the vapor pressures of each component of the mixture and their normal boiling points.


Table 2. Summary of pressure models mentioned in this work.

Model	Mathematical Form	Comment	System	Complexity
Clausius–Clapeyron	$d(\ln P)/d(\frac{1}{T}) = \Delta H_{vap}/R$	Explains temperature dependence	Pure liquids	Very low
Antoine	$\ln P = f(T)$	Three empirically tuned parameters	Pure liquids	Low
Wagner	$\ln(\frac{P}{P_{cr}}) = f(T/T_{cr})$	Four empirically tuned parameters	Pure liquids	Low
Equation of State	Many versions from Van der Waals to Span–Wagner		Gases, but extendable	High
Raoult’s Law	$P_i(T) = x_{i,liq} * P_i^0(T)$	Fundamental	Liquid mixtures	Very low
Wilson	$P_i(T) = a_i * x_{i,liq} * P_i^0(T)$	Tunable activity coefficient (a_i)	Specific liquid mixtures	Data required
UNIFAC	$P_i(T) = a_i * x_{i,liq} * P_i^0(T)$	Activity coefficient found from standard inputs	Liquid mixtures	Moderate
This Work	$P_i(T) = x_{i,liq} * P_i^0(T, x_{i,liq})$	Integrated Clausius–Clapeyron to introduce dependence on mole fraction	Liquid mixtures	Low

Materials and Methods

Vapor Pressure Measurement

The Eravap device, manufactured by Eralytics, was used to measure vapor pressure of liquid samples. The device employs factory-installed software to control sample volume, fill temperature and sample temperature as per user-selected test methodology. We considered the ASTM D6378 (ASTM International, 2022b) triple-point expansion method, as well as the Eralytics® LowVP (low vapor pressure) module. For both methods, the sample is pulled into the measuring cell (see Figure 1) via an actuated piston. A pre-set number of rinse cycles are used to saturate the gas in the measuring cell with sample vapor. Upon conclusion of this conditioning operation, the piston is positioned to a depth corresponding to a chamber volume equal to 4 mL. The suction created by moving the piston up to a depth corresponding to 5 mL is responsible for pulling 1 mL of liquid sample into the measuring cell. During the filling process, sensed pressure is monitored to flag potential filling errors. Once the sensed pressure is found to be within 5 kPa of the (air-only) ambient pressure, which was recorded prior to rinsing, a second timer (t_2) is activated, and the first timer (t_1) is stopped. The first timer starts upon opening the inlet valve (see Figure 1) to the sample. In the controller module, called ASTM D6378, the inlet valve is closed when $t_2 = t_1/3$.

The ASTM D6378 module employs four pre-set volumes (the smallest being 4 mL), which are created by moving the piston within the sealed measuring cell (see Figure 1). The slope of pressure (P) multiplied by volume (V) versus V at constant temperature (T) is the vapor pressure of the sample at that temperature. The total number of moles, as well as the number of sample moles, is determined from the ideal gas law, using total pressure and vapor pressure, respectively, as inputs. The number of moles of air is the difference between these two determined quantities. The Eralytics LowVP module differs from the ASTM D6378 module in several ways. Notable differences include longer fill times achieved by decreasing the pressure variation from ± 5 kPa to a lower value ($\sim \pm 0.15$ kPa), implementing a degassing procedure to rid the liquid phase of any trapped bubbles and executing a triple expansion at a temperature higher than the test temperature to determine the number of moles of air in the sealed measuring cell. For further description of this method, readers are referred to the Eralytics User Manual for the Eravap device.

® Eralytics is a registered trademark of Eralytics GmbH, Austria.

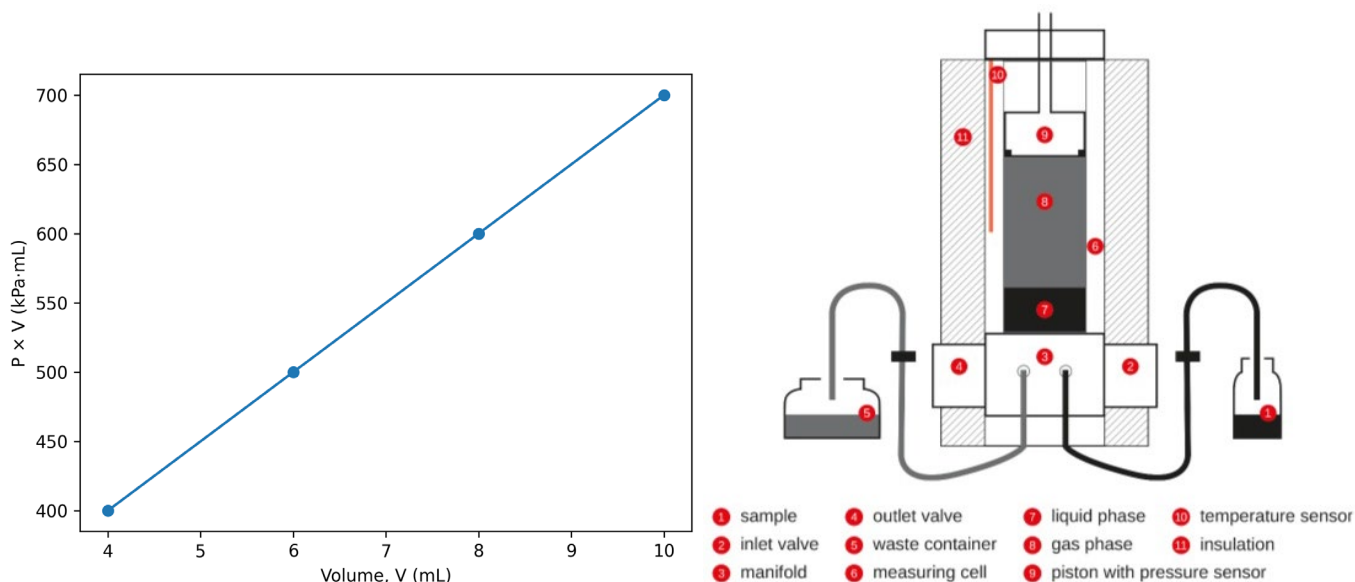


Figure 1. Illustrative ASTM D6378 slope of pressure (P) multiplied by volume (V) vs. V at constant temperature (T) (left), and instrument cross-section (right). Image taken from the Eralytics User Manual for the Eravap device, which is commercially available.

For three pure solvents, n-pentane, toluene and n-decane, the indicated vapor pressure as a function of temperature was compared to reference data published by the National Institute of Standards and Technology (NIST; Linstrom & Mallard, 2001). When using the ASTM D6378 module, we found discrepancies of ± 1.5 kPa, which is much higher than desired for this work. For this reason, we selected the Eralytics LowVP module for all vapor pressure determinations reported here. According to Eralytics, this method has a repeatability of ± 0.15 kPa for all samples at temperatures between -20°C and 120°C , with a vapor pressure between 1.0 kPa and 1000 kPa. Our observations are consistent with the quoted repeatability value.

Materials and Temperatures

The solvents listed in Table 3 were used to make a variety of mixtures containing 0–10%_{mol} of light components. The heaviest component (n-dodecane or n-tetradecane) used in two- or three-component mixtures was present at higher concentration.



Table 3. Materials used in hydrocarbon mixtures. TCD: Trinity College Dublin; WSU: Washington State University.

Name	Normal Boiling Point, °C [29]	Supplier	Purity (%)
n-pentane	36.0	Thermo Scientific	99
cyclohexane	80.8	Fisher Scientific	99.8
n-heptane*	98.4	Alpha Aesar	99
Isooctane	99.2	Sigma Aldrich	99.5
Toluene	110.6	Thermo Scientific	99.7
ethylbenzene*	136.2	Thermo Scientific	99
o-xylene	143.8	TCI	98
n-nonane*	150.6	Thermo Scientific	99
n-propylbenzene*	158.8	Alpha Aesar	98
n-decane*	174.1	Thermo Scientific	99
n-dodecane (TCD)	216.3	Thermo Scientific	99
n-dodecane (WSU)*	216.3	Thermo Scientific	99
n-tridecane*	233.8	TCI	99
n-tetradecane	249.8	Thermo Scientific	99

*These seven materials were part of a 10-component mixture that was distilled as part of this project. The data pertaining to that distillation are available by request to the correspondence author.

Binary mixtures of n-pentane or toluene in n-dodecane, each at four different blending ratios and heated to 70° or 100°C, were used to determine the tuning parameter(s), c . Both sets of binary mixtures included 0.04, 0.06 and 0.09 mole fractions of the lighter component, while the n-pentane/n-dodecane set also included one mixture with a 0.02 mole fraction of n-pentane, and the toluene/n-dodecane set also included one mixture with a 0.06 mole fraction of toluene. A significant difference in volatility was deliberately chosen to minimize the impact of errors stemming from the vapor-liquid equilibrium of the solvent, focusing instead on a single volatile component at low mole fractions. For example, the liquid mixture containing 0.04 mole fraction toluene produces a vapor at 100°C that consists of at least 60% toluene, with wide variation depending on which model is used to predict the component vapor pressures.

Ternary mixtures of n-pentane, toluene and n-dodecane were used as a first level of model validation. In these mixtures, the mole fractions of toluene and n-pentane were made equal to each other: 0.01, 0.04, 0.07 and 0.09. At minimum, the model developed in this work should predict the vapor pressure of these mixtures at 70 and 100°C more accurately than any of the general models, regardless of its relative simplicity, because its parameters were trained specifically on n-pentane and toluene data. Extension of this model to higher temperatures, corresponding to the ambient-pressure bubble points, is somewhat more stressful, but each of the models considered in detail here employ the same vapor pressure curves of the pure components, so even here, the model developed in this work should be more accurate than Raoult's Law and the correction to it based on UNIFAC-determined activity coefficients.

Ternary mixtures, (cyclohexane, o-xylene, n-tetradecane) and (isooctane, o-xylene, n-tetradecane), were used to evaluate the generality of the model. In one experiment, the pot temperature of a mixture made from 2.55 g of cyclohexane, 2.56 g of o-xylene and 44.99 g of n-tetradecane was compared with the modeled liquid temperature of a system for which 0 or 1.0%_{vol} of the liquid is assumed to have vaporized, but to be present in the reflux apparatus (Figure 2) above the surface of the boiling liquid and below the condenser. In another experiment, 100 mL of a mixture made from A (10.36 g of cyclohexane, 10.04 g of o-xylene and 90.93 g of n-tetradecane) or B (10.02 g of isooctane, 10.01 g of o-xylene and 79.96 g of n-tetradecane) was distilled according to the method described as ASTM D86. A brief description of this experiment is provided in the section below under the "Distillations" heading.

Finally, data were extracted from the work of Hung et al. (2024). Although none of the 90 (T, P) vapor-liquid equilibrium points they measured satisfy our predetermined filter criteria, the dataset serves as a valuable benchmark for assessing



how our model performs when applied to systems clearly outside the training set's range. For the record, our predetermined filter criteria were non-associated components, $a < 0.10$ mole fraction of the volatile component(s), which we call solute, $a > 100K$ difference between the solute and solvent's normal boiling points, and a mixture vapor pressure between 1.5 and 101.3 kPa. Their study involved five sets of binary mixtures involving n-nonane, n-octane, methylcyclohexane and methylcyclopentane and three fixed temperatures (120°, 160°, 200°C). We selected the points at 120°C to minimize the confounding effects of real gas behavior, as model (3d) does not address heterogeneous intermolecular attractions/repulsions in the gas phase. Three older datasets by different authors were also evaluated, but the data contained in those reports, relative to Raoult's Law predictions, showed deviations much different from our observations, leading us to question whether we properly understand the experiment they conducted.

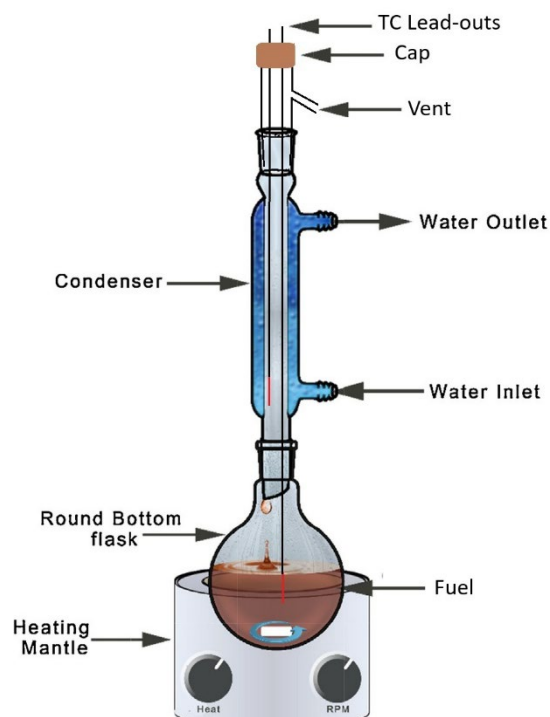


Figure 2. Apparatus used for reflux experiment.

Reflux Experiment

The glassware shown in Figure 2 was used to measure the liquid temperature of a boiling mixture. Type K thermocouples ($\pm 2.2^\circ\text{C}$) were used to measure temperature. Fifty milliliters of a cyclohexane/o-xylene/tetradecane mixture were inserted into the 100 mL round-bottom flask and heated until a steady-state reflux was established. Ordinary tap water was used as the coolant, fed through the condenser sleeve from the bottom port upward, through the top port. Negligible pot temperature (lower thermocouple) variation was observed as the heat flux (vigorousness of the boil) varied. However, the condensate temperature (upper thermocouple) varied significantly with heat flux, with subtle changes in its vertical position. For this reason, the upper thermocouple temperature is not reported here, although it was used to verify internal coherence. For the purpose of comparing the measured liquid (pot) temperature with the theoretical bubble point of the liquid mixture, the dynamic holdup was approximated to contain the equivalent of 1%_{vol} of the sample, or 0.5 mL at reference (lab) temperature. The theoretical temperature corresponding to 1%_{vol} distilled was compared with the measured pot temperature. Additionally, the measured temperature corresponding to the first visual observation of bubbles was recorded, as well as the bubble point, as predicted by the vapor pressure model. In this way, there is a band represented for both the measured and modeled temperatures.



Distillation

Distillations were carried out with the apparatus shown in Figure 3, achieving a collection rate of 1.5–3.0 mL/min from 5% distilled to 50% distilled, which is lower than the requirement stated in ASTM D86 (4–5 mL/min). As a consequence, the degree of separation attained in this set-up is likely somewhat higher than is typical of apparatuses used in conjunction with ASTM D86. The vertical placement of the thermocouple junction is controlled by its sub-assembly, which fits into the ground-glass fitting at the top of the column. Its depth was determined from prior work, manually tuned to reproduce the distillation curve determined with a commercial apparatus conforming fully to the specifications of ASTM D86. The condenser arm is water-cooled, and the collection cylinder is bathed in quiescent air at ambient temperature and pressure. The only vent in the distillation apparatus is at the exit of the condenser arm. Heat is applied via an electrically controlled hot-plate to the bottom of a 125 mL round-bottom flask, which is filled initially with 100 mL of sample. The dimensions of the distillation column, condenser and collection cylinder (100 mL, graduated) are similar to those of the corresponding pieces as specified in ASTM D86. No fractionating media is present in the column.

The volume of dynamic holdup (which includes all mass, liquid or vapor that is not present as liquid in the pot or collection cylinder) varies with the temperature gradient (Ferris & Rothamer, 2016) between the bubble point of the liquid phase (in the pot) and the dew point of the vapor phase at the inflection point in the condenser arm, as well as at the heat flux applied to the bottom of the round-bottom flask. By adjusting the heating rate periodically to maintain a distillate collection rate of 1.5 to 3.0 mL/min, the variation in dynamic holdup throughout the course of the distillation is reduced. The dynamic holdup volume is the largest source of mismatch between the recorded distillation curve temperatures (T_n) and the actual distillate temperature throughout a distillation. It can be anywhere from 0.5 to 10 mL, depending on sample composition (Ferris et al., 2016), but is more commonly approximately 2.6 mL.



Figure 3. Apparatus used for distillations.



Larger dynamic holdup volumes suggest a higher degree of fractionation, because liquid that forms upstream of the inflection point on the condenser arm will drain toward the heat and re-vaporize (whether fully or partially) prior to blending back into the pot. Bounding assumptions of one or two theoretical plates of separation are assumed here for the purpose of comparing modeled distillations with measured distillation curves and distillate compositions. The theoretically estimated temperatures should be consistently higher than the measured temperatures (T_n) if they accurately reflect the actual temperature of a system with $n\%$ 'not-in-pot,' which includes dynamic holdup volume and collection volume, instead of $n\%$ collected.

The fraction distilled is defined as the volume of distillate collected, divided by the volume of sample charge, which is 100 mL. The temperature can be monitored throughout the distillation, although usually the operator will only record the temperature at pre-determined distillate volumes. For example, at 10%_v distilled, the operator may record T10 if 10%_v is a pre-determined test point. In this work, the operator has recorded four points for distillation of the ternary mixture (T5, T10, T15 and T20). Specific to this work, a 0.2 mL sample of distillate was pipetted from the collection cylinder at each of the scheduled test points for the purpose of characterizing its composition via two-dimensional gas chromatography (GCxGC)/flame ionization detector (FID). The composition of distillate is not subject to errors introduced by the dynamic holdup. To minimize distillate sample inhomogeneity, the material in the graduated cylinder was swirled and agitated by pulsing with five pipette volumes prior to each collection, and to minimize the risk of evaporative loss from the sample, it was immediately transferred to the gas chromatograph. The sampled volumes were not compensated for later collections, meaning the actual collected distillate volume at the second test point, for example, was 0.2 mL greater than indicated by the test point schedule, which consistently referenced the volume of material in the graduated cylinder.

Distillate Composition Analyses

The composition of each distillate was determined by two-dimensional gas chromatography with an in-series FID, according to the method described originally by Striebich et al. (2014) and later by Trinklein et al. (2020). In these experiments, the composition determination was particularly simple because the samples were made of just three highly pure components that eluted over easily distinguished time/time domains.

One micro-liter of undiluted sample was injected into the head of the gas chromatograph. The integrated FID response corresponds to the mass of each component that elutes over the user-defined time domain of the integration. Since all masses are determined, and the identity of all species are known in advance, the corresponding mass, mole or volume fractions of each component can be readily determined.

Modeled Distillation

Idealized one-plate and two-plate distillations were completed for each experimentally distilled mixture and each vapor pressure model (this work and Raoult's Law). The initial condition is 100 mL of a test mixture of a known composition at ambient temperature and pressure (P_{amb}), from which total moles are determined. This mixture is heated (or cooled) in increments of 0.001K until its vapor pressure reaches ($P_{amb} \pm 0.001$) kPa. At that point, for one-plate distillations, 0.1%_{mol} of material, with its composition determined by the modeled vapor phase, is removed from the system. The dew point of this drop is determined by cooling (or heating) the vapor in increments of 0.001K until a liquid of that composition produces a vapor pressure of ($P_{amb} \pm 0.001$) kPa. For two-plate distillations, two vapor-phase compositions are tracked. The first one (the higher-temperature one) is determined by the temperature and composition of material in the pot; and the second one (the lower-temperature one) is determined by the temperature and composition of the first drop. The second bubble point temperature is equal to the first dew point temperature. This temperature, along with the composition of the first drop (as well as the first vapor phase), determines the composition of the second phase. At this point, for two-plate distillations, 0.1%_{mol} of material, with its composition determined by the second modeled vapor phase, is removed from the system. The dew point of this (second) drop is determined by cooling (or heating) the vapor in increments of 0.001K until a liquid of that composition produces a vapor pressure of ($P_{amb} \pm 0.001$) kPa. In each case the modeled (final) dew point is compared with experimentally measured condensate temperatures.

To model a significant span of the distillation curve, this process is repeated up to 1,000 steps, with an incremental reduction in liquid in the pot at each step. To avoid numerical issues that are likely to arise somewhere (between 950 and 1,000 steps) as the quantity of material being extracted becomes significant relative to the total material left in the system, we stop the numerical distillations at 950 steps. The (first) bubble point temperature, (final) dew point temperature and composition of the extracted drop are recorded at each step. The fully mixed distillate composition is also updated at each step.



Results

Tuning Vapor Pressure Models

The mixtures of n-pentane in n-dodecane and toluene in n-dodecane were used to represent the vapor pressure of an aliphatic or aromatic solute dissolved in a hydrocarbon solvent. A large volatility difference between the solute and solvent was chosen so that the composition of the vapor phase would be predominantly one component, the solute, even as the solute mole fraction in the liquid phase was taken down to 0.02 (n-pentane) or 0.04 (toluene). Thus, the confounding impact of solvent vapor pressure was minimized. Table 4 documents the normal boiling points and the Antoine coefficients for each of these three materials, where the Antoine equation was used to obtain the values of $P_{vap,i}$ that were used in Equation 2. The singularity (in Equation 2) that occurs when the temperature equals the normal boiling point does not arise at the tuning stage of this work because only test temperatures (70° and 100°C) not equal to the normal boiling point of any component were selected. Two values of temperature were chosen, effectively decoupling variation in $E_{a,i}$ from normal boiling point variation. A mix of aliphatic and aromatic hydrocarbons (one each) was deliberately selected because the entropy of vaporization, which effectively relates to the normal boiling point temperature and the heat of vaporization, is somewhat different for each; approximately 86.5 and 72.5 J/mol/K for alkanes and aromatics, respectively. Our intent here is to model each in the same way and to assess the error introduced by neglecting this difference. For reference, the approximate entropies of vaporization of cycloalkanes and alkenes are 85.0 and 82.5 J/mol/K, respectively, within the bounds of the representatives chosen for this work.

Table 4. Antoine coefficients of selected materials: $\log_{10}(P) = A - B / (T + C)$.

Material	nBP (°C)	A	B (K)	C (K)
n-pentane	36.0	3.9892	1070.617	-40.454
toluene	110.6	4.0783	1343.9	-53.77
n-dodecane	216.3	4.10549	1625.928	-92.839
cyclohexane	80.8	3.96988	1203.526	-50.287
o-xylene	143.8	4.12928	1478.244	-59.076
n-tetradecane	249.8	4.13735	1739.623	-105.616
isooctane	99.2	3.9368	1257.8	-52.42

For the n-pentane/n-dodecane mixtures, vapor pressure data were recorded for mixtures with 2, 4, 6 and 9%_{mol} n-pentane at 70° and 100°C. For the toluene/n-dodecane mixtures, vapor pressure data were recorded for mixtures with 4, 6, 8 and 9%_{mol} toluene at 70° and 100°C. These 16 data points were used to train the models. Figure 4 displays the best fit for each of the models defined in Equations 3a-3d. The toluene/n-dodecane data are confined to panel (a) and the n-pentane/n-dodecane data are confined to panel (b). The motivation for showing all of these fits is to underscore the improvement offered by the second tuning parameter. For model (3d), the root mean square and mean absolute errors are 0.35 and 0.25 kPa, respectively, substantially better than any of the single-parameter models. More importantly, for model (3d), the error is split evenly between each of the four groupings of data, resulting in a mean error of just 0.09 kPa and a mean absolute relative error (MARE) of 3.5%. In contrast, the errors of the single-parameter models are heavily skewed toward the toluene/n-dodecane mixtures, while a temperature-dependent pattern is also apparent. The tuned values of s , applicable to model (3d), are reported in Equations 5 and 6.

$$C(x_i) = T_{ref,i}^0 (1.0154 - 0.0154 \times x_i) \quad (\text{Eq. 5})$$

$$B(x_i) = E_{a,i}^0 (0.77275 + 0.22725 \times x_i) \quad (\text{Eq. 6})$$

A comparison of model (3d) with other global models, UNIFAC and Raoult, is displayed in Figure 5. Surprisingly to these authors, the zero-parameter Raoult's Law misrepresents the n-pentane/n-dodecane vapor pressures at 100°C by a whopping 22% to 60%, while it essentially matches the toluene/n-dodecane vapor pressures at 100°C. Across the 16 points, its MARE is 26.6%. Compared with the 100°C data, at 70°C, Raoult's Law predictions decrease relative to the data for both sets of mixtures, which is a characteristic shared by the UNIFAC model predictions. The "corrections" to Raoult's Law offered by the UNIFAC activity coefficients scale the vapor pressures of the toluene/n-dodecane mixtures (activity



coefficients > 1) to higher values, which drives it in the wrong direction at 100°C and the right direction at 70°C . For the n-pentane/n-dodecane mixtures, the UNIFAC model (activity coefficients < 1) scales Raoult's Law vapor pressures to lower values, which is closer to the data at both 70° and 100°C , but still wrong by up to 31% at 100°C for the mixture containing 9.0% $_{\text{mol}}$ n-heptane. Across the 16 points, its MARE is 12.6%. Clearly, the two-parameter model developed here shows greater promise than the activity coefficient approach represented here by the UNIFAC model, which has a total of seven tuned parameters that are applicable to these mixtures.

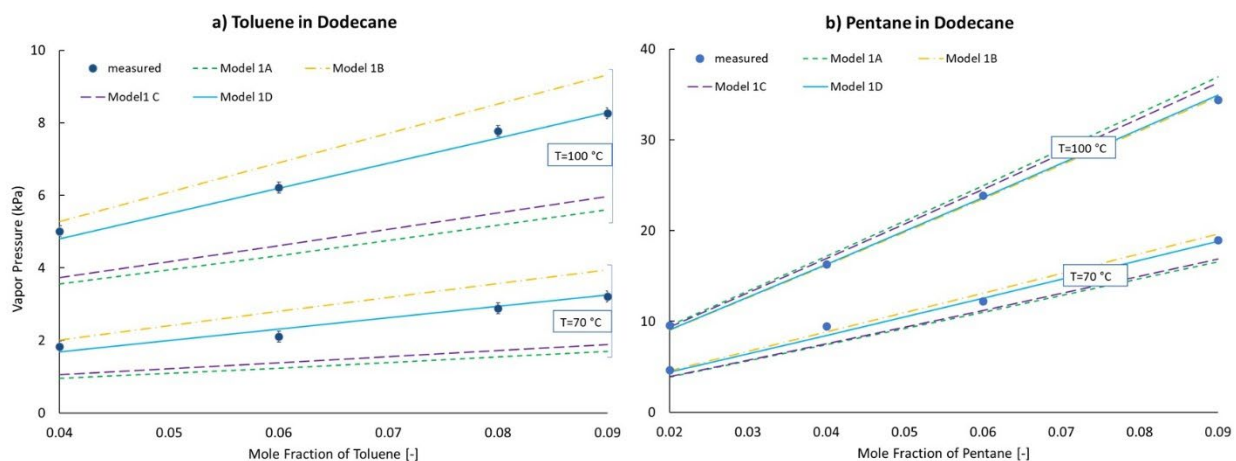


Figure 4. Vapor pressure model tuning results. Filled symbols correspond to measurements. Curves correspond to model predictions.

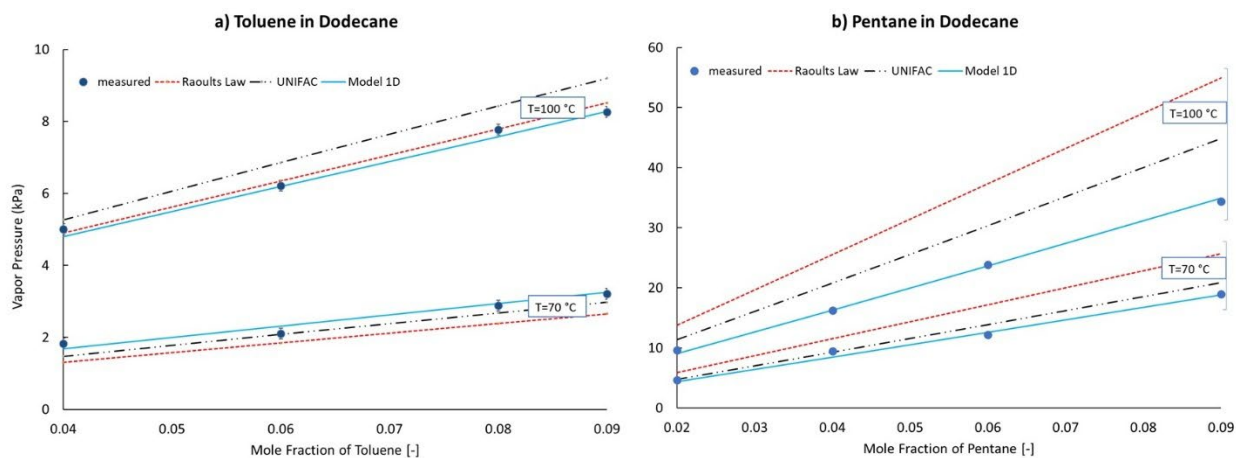


Figure 5. Tuned vapor pressure model comparisons. Filled symbols correspond to measurements. Curves correspond to model predictions.

Modeled Vapor Pressure Validation

The first level of validation discussed is to compare predictions to measurements of systems under slightly different conditions compared with the tuning dataset. Here we use ternary mixtures of n-pentane, toluene and n-dodecane. For convenience of reporting, the mole fractions of toluene and n-pentane were prepared equal to each other. According to Raoult's Law and model (3d), the vapor pressure of this mixture should be essentially the sum of the vapor pressures of



the respective binary mixtures, because these models do not consider potential differences between components of differing identities, and the slight reduction in n-dodecane's contribution to the total vapor pressure is small, because its vapor pressure is much lower than those of n-pentane and toluene. In contrast, the activity coefficients of the UNIFAC model are impacted by the identities of the other components. For example, at 9%_{mol}, the activity coefficient of n-pentane is 0.811 at 70°C for the binary mixture and 0.837 for the ternary mixture. Very astute readers may be able to see the effect of this difference by comparing Figure 5 and Figure 6, as the UNIFAC model is slightly more wrong for the ternary mixture than the binary mixture at this temperature, even though it gets the vapor pressure of toluene right at this temperature. Comparison to the equation-of-state (EOS) model (Kunz & Wagner, 2012) used in REFPROP (Lemmon et al., 2013), which lacks key features relevant to complex mixtures such as fuels, reveals several notable observations. Although exaggerated relative to the measured vapor pressure curves, the EOS model predicts some curvature to the vapor pressure as a function of the mole fraction, whereas this characteristic of model (3d) (clearly present based on Equations 5 and 6) is not visibly apparent on the viewing scales of Figures 4-6. The temperature dependence of the EOS model brings it closer to the measured values at 100°C than at 70°C, which may not be surprising, because the critical temperature is a focal point within that model's framework. Most surprising to the authors, however, was the magnitude of the errors afforded by this model in spite of its complexity and specificity to these three materials. In numerical summary, the MAREs of model (3d), Raoult's Law, UNIFAC and REFPROP are 44.6%, 24.3%, 33.6%, and 5.5%, respectively. Only model (3d) has a lower mean relative error (MRE) magnitude (5.1%) than MARE.

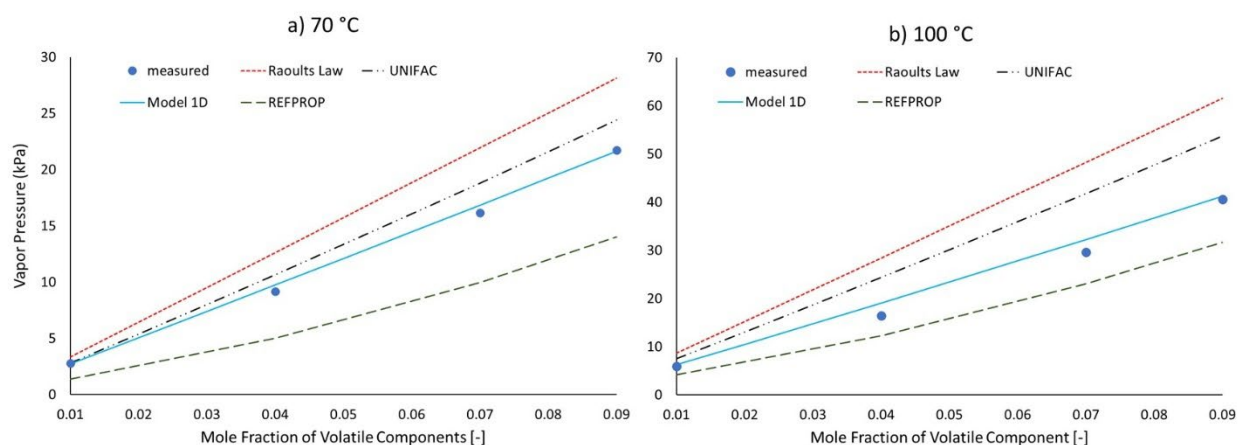


Figure 6. Measured and predicted vapor pressures of ternary mixture. Filled symbols correspond to measurements. Curves correspond to model predictions.

The next level of validation is to introduce a greater variety of materials and temperatures, resulting in vapor pressure up to ambient pressure. One simple way to obtain this data is to measure the temperature of a refluxing mixture. The temperature of the liquid phase is easy to get right, and the pressure is the barometric pressure of the lab, but the composition of the liquid phase is somewhat confounded because some mass of sample exists as dynamic holdup; vapor or condensed vapor that has not yet fallen back into the pot. In Figure 7, we show the measured reflux temperature of a mixture of o-xylene (8.6%_{mol}), cyclohexane (10.8%_{mol}) and tetradecane (80.6%_{mol}) in comparison with the predicted bubble point resulting from model (3d), Raoult's Law and the UNIFAC model. To account for the uncertainty of the liquid-phase composition, predictions corresponding to 0 and 1%_{vol} are reported. The measured temperatures correspond to the moment when the first bubble was observed (bottom) and the moment it reached a steady-state temperature (top). For each of the models, the $P_{vap,i}$ term in Equation 2 was represented by an Antoine equation, with coefficients as documented in Table 4. As is quite evident from Figure 7, model (3d) predicts a normal boiling point and refluxing temperature, in far better agreement with the measured values than Raoult's Law or the UNIFAC model. While none of the models predict the measured result to within the $\pm 2.2^\circ\text{C}$ reproducibility of the thermocouple, the vapor pressure predicted by model (3d) at the lower edge of the measured temperature uncertainty band is just 11% higher than lab pressure, much closer than the other models. The liquid phase composition of 1%_{vol} distilled for both model (3d) and UNIFAC reflux temperatures (upper) was based on model (3d), and one theoretical plate was assumed since no removal of material was occurring in this system.

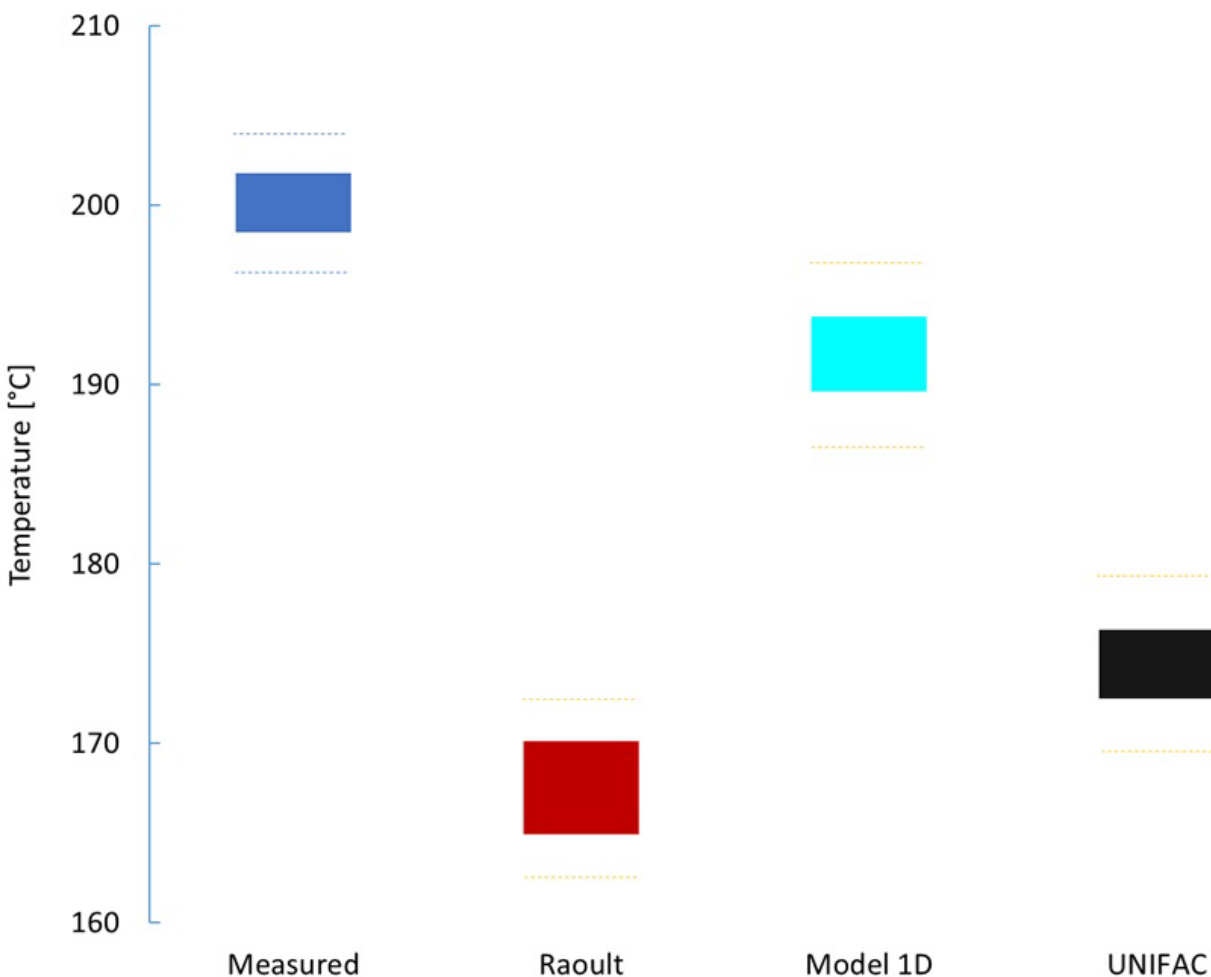


Figure 7. Measured and predicted liquid temperature of a refluxing mixture of cyclohexane and o-xylene in tetradecane. The dashed blue lines correspond to the temperature measurement uncertainty of $\pm 2.2^\circ\text{C}$. The dashed yellow lines correspond to the predicted temperature at a vapor pressure within $\pm 5\%$ of lab pressure.

Literature Data

Recently, Hung et al. (2024) measured and predicted the vapor pressure of 20 different binary mixtures involving n-nonane, n-octane, methylcyclohexane or methylcyclopentane at 120° , 160° , or 200°C (see Figure 8). Their predictions were made via Aspen Plus[®] V11 using COSMO-SAC, UNIFAC-DMD and two additional models with coefficients of binary interactions re-tuned to their measurements and Hayden-O'Connell fugacity coefficients. A description of the UNIFAC-DMD model (highlighting modifications to UNIFAC) was provided by Gmehling et al. (1993), while a description of the COSMO-SAC model was provided by Hsieh et al. (2010). The MAREs of UNIFAC-DMD and COSMO-SAC were 1.5% and 5.1%, respectively. Comparatively, the simple two-parameter model presented here results in a MARE of 5.1% and MRE, or over-prediction, of -0.7%, considering only the data at 120°C to avoid having to account for real gas differences related to an ideal gas. Model (3d) overpredicts the vapor pressure of eleven mixtures while underpredicting the vapor pressure of nine mixtures. In contrast, Raoult's Law over-predicts the vapor pressure of all 20 mixtures, two of them by more than 40%, and has a MARE of 13.7%.

[®] Aspen Plus is a registered trademark of AspenTech Corporation, Bedford, Massachusetts.



It is worth noting here that the performance of model (3d) on this dataset is consistent with the authors original intent, which was to develop an algebraically simple model (suitable for hand calcs, spreadsheets or codes/applications that require vapor pressure or composition many thousands of times per run) that provides much-improved accuracy relative to Raoult's Law while remaining comparatively accurate to the more complicated and mature models used in commercially available applications that serve process engineering and industrial simulations. Model (3d) is not intended to replace models such as UNIFAC but rather to reach applications (through its simplicity) that are not currently pragmatic for UNIFAC. Specifically, this model does not address heterogeneous, real gas effects and should not be applied to conditions where such terms are expected to be important. It can be applied to our research goals, which are to support conceptual-level distillation cut-point optimization, as exemplified by Yang et al.(2023), bubble point prediction in the fuel system at chop from cruise to flight idle, preferential evaporation effects on lean blow at this same (jet engine) operating condition and evaporation rate predictions in (future) simulations of ignition in jet engines. Of these, the only one that is pragmatic for applications like ASPEN is the check on bubble point in the fuel system at the min-thrust/max-altitude (combustor) design point, but jet engine combustor designers do not generally have access to any such commercial application.

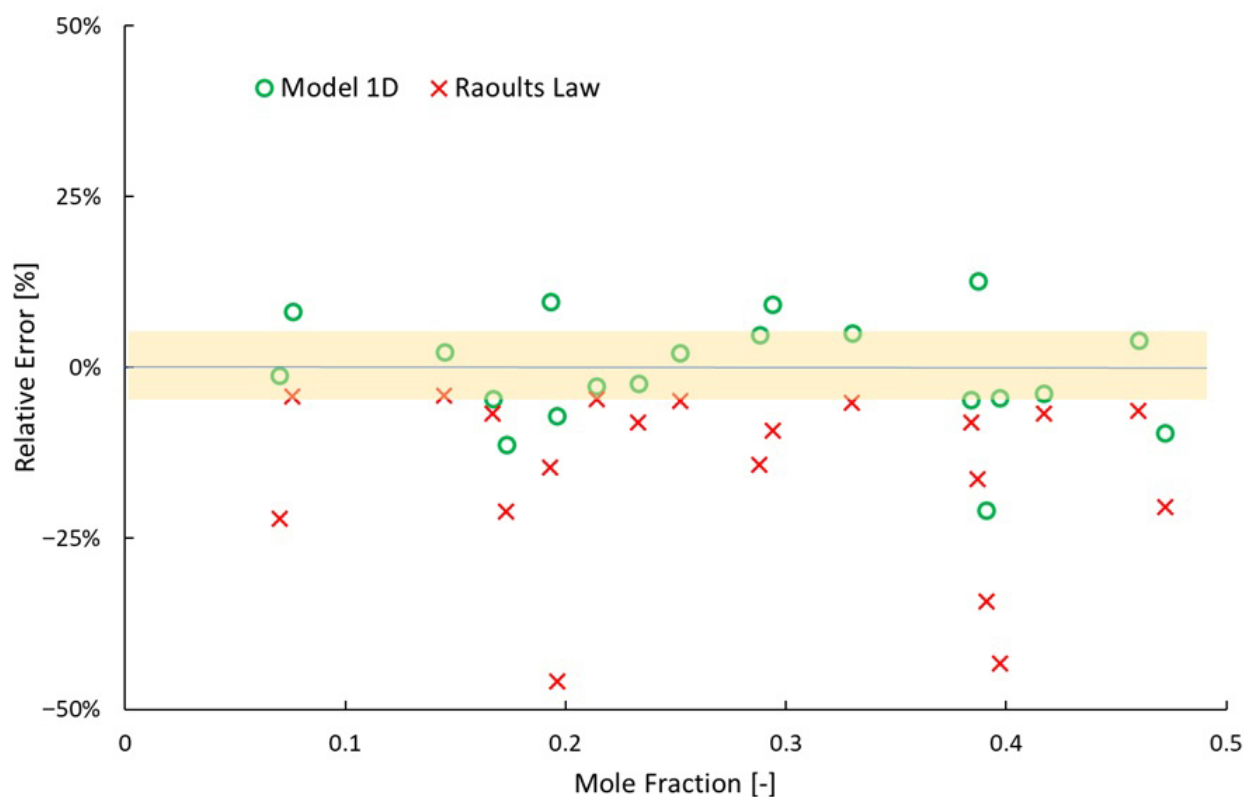


Figure 8. Relative error of vapor pressure predictions of assorted binary mixtures of n-nonane, n-octane, methylcyclohexane or methylcyclopentane. The measurements were taken from the vapor-liquid equilibrium work by Hung et al. (2024). Temperature equals 120°C and pressure equals 45.9–261.1 kPa. Relative error is defined as (measurement–prediction) divided by measurement. The shaded region corresponds to $\pm 5\%$.

Modeled Distillation Validation

The final validation of the vapor pressure model compares predicted distillation curves with measured distillation curves. However, the model of the distillation process may be more important to these curves than the vapor pressure model. Figure 9 is used to compare the measured distillation curve of the ternary blend initially containing 18.2%_{mol} (9.3%_{vol}) cyclohexane and 14.0%_{mol} (7.8%_{vol}) o-xylene, with the balance being tetradecane. Clearly the difference resulting from the variable number of theoretical plates assumed for the distillation, one or two, has a much larger impact on the modeled



distillation curve than the choice of vapor pressure model, Raoult or model (3d). Regardless of vapor pressure model, the assumption of two theoretical plates results in a predicted distillation curve that more closely matches the measured data. Two sets of points are used to represent the measured distillation curve. One set corresponds to the measured temperature at the moment the collected distillate volume equals the first drop, 5 mL, 10 mL, 15 mL and 20 mL. The latter three points are shifted to the right to account for the distillate sample volume removed for later composition analysis. The second set of points accounts for the dynamic holdup volume, which we estimate to be 2.6 ± 1.2 mL. By comparing the curves displayed in panel a) with those displayed in panel b), it is apparent that Raoult's Law predicts more separation between the components for both distillation models; more featured and greater difference between the initial boiling point (IBP) and the temperature at 20%_{vol} distilled (T_{25}). Relative to the measured data, Raoult's Law with two theoretical plates over-separates the mixture while model (3d) under-separates the mixture. An optimized linear combination of the one- and two-plate curves for Raoult's Law and model (3d), respectively, results in a rms error of 12.3 and 9.2°C. The two-plate curve weighting coefficient is 70% for Raoult's Law and 91% for model (3d).

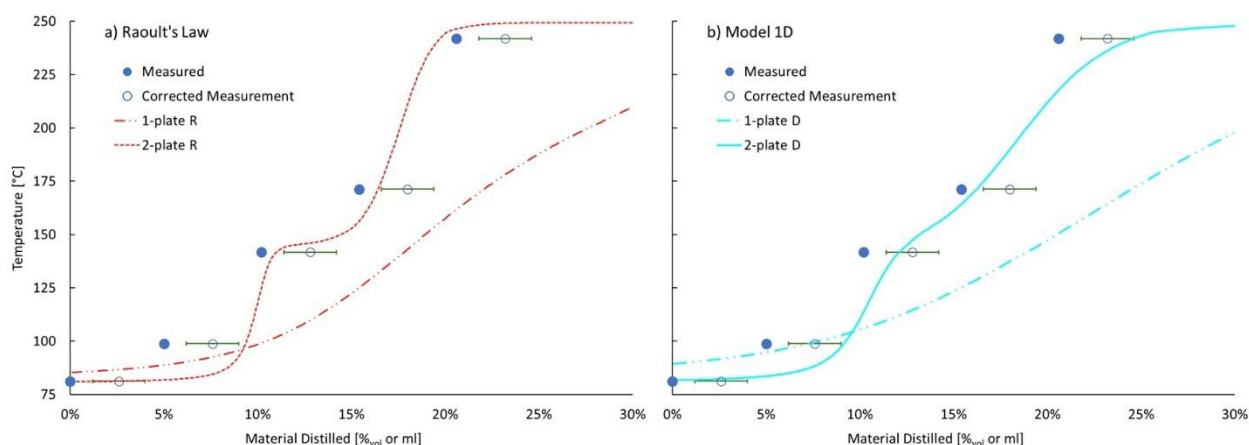


Figure 9. Measured and predicted distillation curve of a mixture of cyclohexane and o-xylene in tetradecane. Filled symbols correspond to measurements. Open symbols correspond to corrected measurements. The uncertainty bars correspond to the range of our estimated dynamic holdup volume. Curves correspond to model predictions.

To gain further insight into which vapor pressure model more accurately represents this distillation process, the measured and predicted distillate composition is compared in Figure 10. The dynamic holdup volume is not applicable to this data. The measured compositions were determined from GCxGC/FID analysis of samples drawn from the collection vessel. To account for the disconnect (1.53 mL) between the total volume of cyclohexane collected and its volume in the initial ternary mixture, we assume it was lost as vapor throughout the distillation. The open symbols in Figure 10 represent the measured data, corrected under this assumption. The vapor loss at each point is scaled by the ratio of liquid cyclohexane collected at each point divided by the final volume of cyclohexane collected. Relative to these points, it is clear that both vapor pressure models, within the two-theoretical-plate distillation model, predict greater separation at the first data point, overrepresenting cyclohexane and underrepresenting both o-xylene and n-tetradecane. By the second data point, when most of the cyclohexane is distilled, both vapor pressure models result in a predicted o-xylene concentration that matches the corrected data. Neither model captures the full extent of n-tetradecane bleed-through into the distillate. The missed n-tetradecane content may seem small in the context of vapor pressure, but the freeze point of this distillate is determined by n-tetradecane, where a mole fraction of 1% is expected result in a freeze point of -40°C (Bell et al., 2025). The difference between a measured mole fraction of 1.9% and a predicted mole fraction of 0.7% (or less) is the difference between having a product that will pass inspection or fail inspection. While model (3d) with two theoretical plates of separation is closer to reality than Raoult's Law with two theoretical plates, this distillation experiment falls somewhat short of two theoretical plates. The symbol x in Figure 10 corresponds to the prediction that weights a two-plate distillation by 70% and 91% for Raoult's Law and model (3d), respectively. The agreement between the measured distillate composition and its prediction based on model (3d) with two plates of separation weighted by 91% and one plate of separation weighted by 9% is remarkable at 5%, 10%, and 15% distilled, but at 20% distilled, it under-predicts o-xylene concentration while over-



predicting n-tetradecane concentration. In contrast, the modeled distillation based on Raoult's Law vapor pressures with 70% two-plate separation and 30% one-plate separation is wildly inconsistent with measured distillate composition at 15% and 20% recovered.

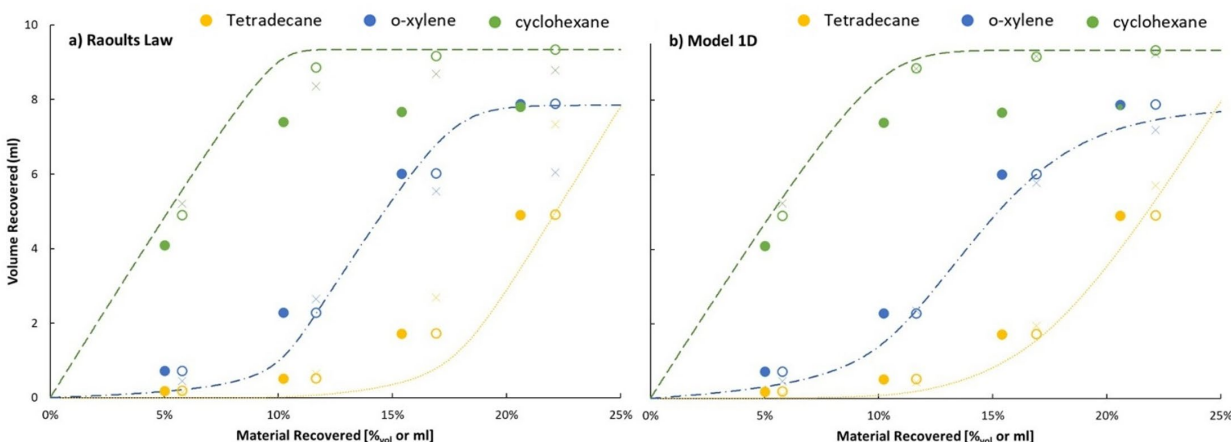


Figure 10. Measured and predicted distillate composition of a mixture of cyclohexane and o-xylene in tetradecane. Filled symbols correspond to measurements. Open symbols correspond to corrected measurements. Curves and \times symbols correspond to model predictions. Green symbols and curves correspond to cyclohexane. Blue corresponds to o-xylene. Yellow corresponds to n-tetradecane.

In order to reduce the confounding effect of evaporative losses, a second ternary mixture was distilled. This mixture initially contained 15.0%_{mol} (11.1%_{vol}) isooctane and 16.1%_{mol} (8.6%_{vol}) o-xylene, with the balance being tetradecane. A comparison between the measured distillation curve and its prediction based on model (3d) vapor pressures and a two-plate distillation or a 96% two-plate plus 4% two-plate distillation is provided in Figure 11. The rms error of the weighted distillation curves is 10.5°C, stemming almost entirely from the big miss at 15% to 20% distilled, where the recorded temperature (130.9°C) is substantially less than the normal boiling point of o-xylene (143.8°C). The measured and modeled distillate compositions are displayed in Figure 12. Consistent with the previous result, the predicted recovery of o-xylene is noticeably under-represented by the model, while isooctane is over-represented at all four points of comparison, and n-tetradecane content is over-represented by the model at 20% recovery.

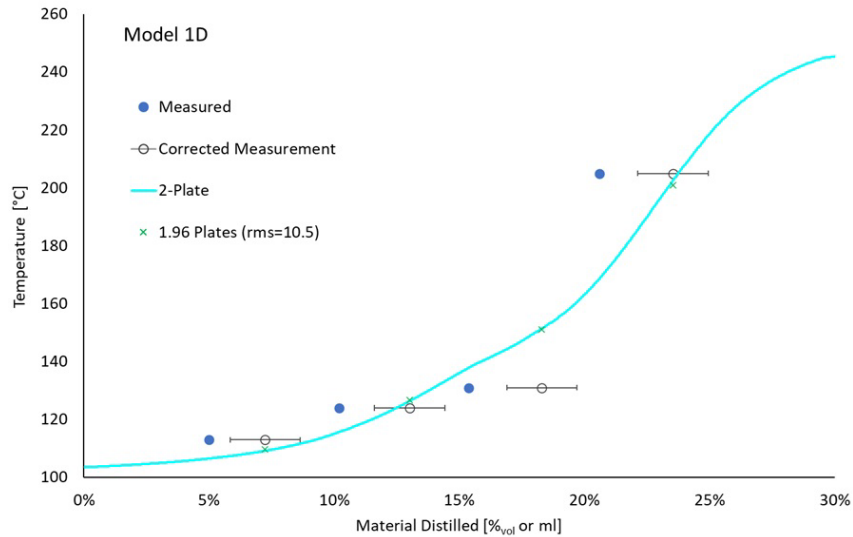


Figure 11. Measured and predicted distillation curve of a mixture of isooctane and o-xylene in tetradecane. Filled symbols correspond to measurements. Open symbols correspond to corrected measurements. The uncertainty bars correspond to the range of our estimated dynamic holdup volume. Curves and x symbols correspond to model predictions.

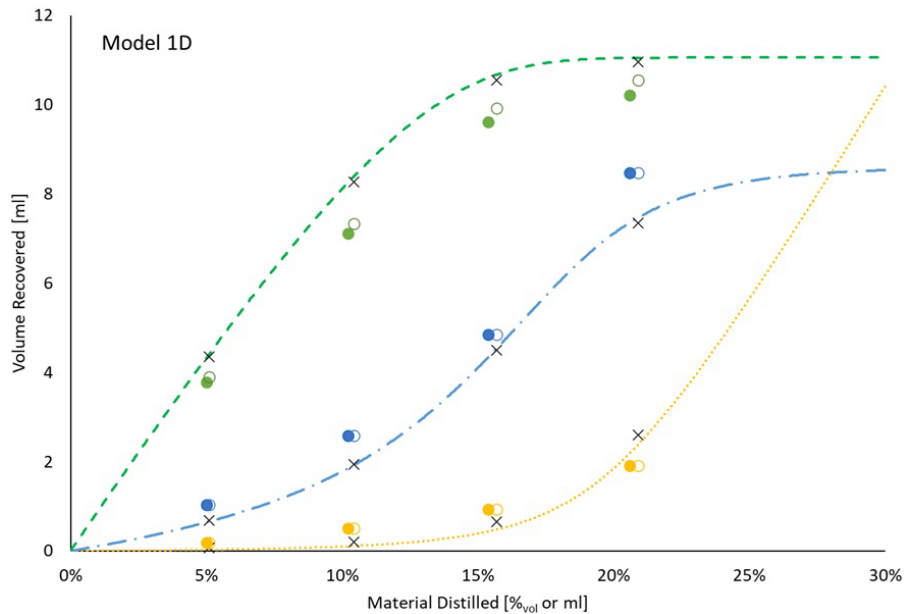


Figure 12. Measured and predicted distillate composition of a mixture of isooctane and o-xylene in tetradecane. Filled symbols correspond to measurements. Open symbols correspond to corrected measurements. Curves and x symbols correspond to model predictions. Green symbols and curves correspond to isooctane. Blue corresponds to o-xylene. Yellow corresponds to n-tetradecane.

Conclusions

A global two-parameter vapor pressure model that is rooted in our physical understanding of evaporation of hydrocarbon mixtures has been developed. Sixteen vapor pressure measurements involving two different temperatures, two binary



systems and four concentrations were used to tune the parameters, which were used to scale both the activation energy (or heat of vaporization) term and reference temperature term in the Clausius-Clapeyron equation as a function of the mole fraction.

Comparisons to 29 points ($T, P, \{x_i\}$) and four temperature curves have been presented, showing dramatically better accuracy relative to Raoult's Law and comparable accuracy relative to the UNIFAC model. Additionally, two comparisons between measured and predicted distillation curves and distillate compositions of two different ternary mixtures further demonstrate that the simple vapor pressure model presented here outperforms Raoult's Law, but these comparisons also highlight the fact that modelling the distillation process is challenging.

The confounding of distillation process modeling errors with vapor pressure (and vapor composition) modeling errors makes it difficult to validate either from data collected during a distillation experiment. To get around this issue and the uncertainty it causes, crude oil (whether synthetic or petroleum in origin) refiners may employ somewhat more fractionation than necessary, which also desensitizes the process to vapor pressure model accuracy. Alternatively, mature yet computationally extensive options available through Aspen Plus, DWSIM or ChemCAD may offer more accurate process simulations, but it would be impractical to put such tools within the inner-most loop of decision logic to select the cut points of crude oil refinement, and essentially impossible to nest them into computational fluid dynamics simulation of evaporation under combustor operating conditions near ignition, lean blow out or any other important combustor operating point. The model presented here provides dramatic improvement relative to Raoult's Law, with a very modest increase in computational complexity.

Milestone

Performed distillation optimization for eight SAF candidates from six different pathways.

Major Accomplishments

Developed a new vapor pressure model to capture molecules with low concentrations to improve distillation optimization model.

Publications

Yang, Z., Bell, D. C., Cronin, D. J., Boehm, R., Heyne, J., & Ramasamy, K. K. (2024). Volatility measurements of sustainable aviation fuels: a comparative study of D86 and D2887 methods. *ACS Sustainable Chemistry & Engineering*, 12(19), 7414-7420. <https://doi.org/10.1021/acssuschemeng.4c00678>

Yu, S., He H., Summers, S., Yang, Z., Si, B., Heyne, J., Zhang, Y., Yang, H. (2025). Upgrading of biocrude oil into sustainable aviation fuel using molybdenum carbide nanocatalysts, *Science Advances*. 11(26), 5777. <https://doi.org/10.1126/sciadv.adu5777>

Boehm, R., Parker, R., Yang, Z., Dooley, S., & Heyne, J. (2025). Blend Prediction Model for Vapor Pressure of Jet Fuel Range Hydrocarbons. *Sustainability*, 17(21), 9612. <https://doi.org/10.3390/su17219612>

Outreach Efforts

None.

Awards

Joshua Heyne - 2024 Energy and Fuels Rising Starts

Student Involvement

Washington State University PhD student, Alexander Kelly, leads this effort.

Plans for Next Period

- Continue improvement on the distillation optimization tool and procedure with the new vapor pressure model.
- Coordinate with novel fuel producers to optimize their distillation process.

References

Antoine, M. C. (1888). Nouvelle relation entre les tensions et les temperatures. *Seanc. Acad. Sci.*, 107, 681-684.



- ASTM International. (2022a). ASTM D7566-21: Standard Specification for Aviation Turbine Fuel Containing Synthesized Hydrocarbons. <https://doi.org/10.1520/D7566-21>
- ASTM International. (2022b). ASTM D6378-22: Standard Test Method for Determination of Vapor Pressure (VPX) of Petroleum Products, Hydrocarbons, and Hydrocarbon-Oxygenate Mixtures (Triple Expansion Method). <https://doi.org/10.1520/D6378-22>
- ASTM International. (2023a). ASTM D1655-25a: Standard Specification for Aviation Turbine Fuels. <https://doi.org/10.1520/D1655-25A>
- ASTM International. (2023b). ASTM D4054-22: Standard Practice for Evaluation of New Aviation Turbine Fuels and Fuel Additives. <https://doi.org/10.1520/D4054-22>
- ASTM International. (2024a). ASTM D86-23: Standard Test Method for Distillation of Petroleum Products and Liquid Fuels at Atmospheric Pressure. <https://doi.org/10.1520/D0086-23>
- ASTM International. (2024b). ASTM D2887-23: Standard Test Method for Boiling Range Distribution of Petroleum Fractions by Gas Chromatography. <https://doi.org/10.1520/D2887-23>
- Bell, D. C., Boehm, R., & Heyne, J. S. (2025). Freezing Point of Hydrocarbon Fuels from Single Species Concentrations. *Energy Fuels*, 39, 4221–4226. <https://doi.org/10.1021/acs.energyfuels.4c06091>
- Clapeyron, P. E. (1834). Memoire sur la Puissance Motrice De La Chaleur. J. L'école Polytech/Publié Par Le Cons D'instruction Cet Établissement. <https://gallica.bnf.fr/ark:/12148/bpt6k4336791/f157>
- Clausius, R. (1850). Ueber die bewegende Kraft der Wärme und die Gesetze, welche sich daraus für die Wärmelehre selbst ableiten lassen. *Annalen der Physik*, 155(4), 500–524. <https://doi.org/10.1002/ANDP.18501550403>
- Côcco, L. C., Yamamoto, C. I., & Von Meien, O. F. (2005). Study of correlations for physicochemical properties of Brazilian gasoline. *Chemometrics and Intelligent Laboratory Systems*, 76(1), 55–63. <https://doi.org/10.1016/j.CHEMOLAB.2004.09.004>
- Colket, M., & Heyne, J. (2021). Progress in Astronautics and Aeronautics. In *Fuel Effects on Operability of Aircraft Gas Turbine Combustors*. The American Institute of Aeronautics and Astronautics, Inc., Reston, Virginia. <https://doi.org/10.2514/4.106040>
- Cooper, J. B., Wise, K. L., Groves, J., & Welch, W. T. (1995). Determination of Octane Numbers and Reid Vapor Pressure of Commercial Petroleum Fuels Using FT-Raman Spectroscopy and Partial Least-Squares Regression Analysis. *Analytical Chemistry*, 67(22), 4096–4100. <https://doi.org/10.1021/ac00118a011>
- Crozier, P. S., & Rowley, R. L. (2002). Activity coefficient prediction by osmotic molecular dynamics. *Fluid Phase Equilibria*, 193(1-2), 53–73. [https://doi.org/10.1016/S0378-3812\(01\)00734-8](https://doi.org/10.1016/S0378-3812(01)00734-8)
- EASC. (1974). GOST 20227-74: Medical elastic bandages, Method for determination of ductility. Euro-Asian Council for Standardization, Metrology and Certification.
- Ferris, A. M., & Rothamer, D. A. (2016). Methodology for the experimental measurement of vapor–liquid equilibrium distillation curves using a modified ASTM D86 setup. *Fuel*, 182, 467–479. <https://doi.org/10.1016/j.fuel.2016.05.099>
- Flecher, P. E., Welch, W. T., Albin, S., & Cooper, J. B. (1997). Determination of octane numbers and Reid vapor pressure in commercial gasoline using dispersive fiber-optic Raman spectroscopy. *Spectrochimica Acta Part A: Molecular and Biomolecular Spectroscopy*, 53(2), 199–206. [https://doi.org/10.1016/S1386-1425\(97\)83026-0](https://doi.org/10.1016/S1386-1425(97)83026-0)
- Flumignan, D. L., de Oliveira Ferreira, F., Tininis, A. G., & de Oliveira, J. E. (2008). Multivariate calibrations in gas chromatographic profiles for prediction of several physicochemical parameters of Brazilian commercial gasoline. *Chemometrics and Intelligent Laboratory Systems*, 92(1), 53–60. <https://doi.org/10.1016/j.CHEMOLAB.2007.12.003>
- Fredenslund, A., Jones, R. L., & Prausnitz, J. M. (1975). Group-contribution estimation of activity coefficients in nonideal liquid mixtures. *AIChE Journal*, 21(6), 1086–1099. <https://doi.org/10.1002/aic.690210607>
- Gaudin, T., & Ma, H. (2020). The macroscopic viscosity approximation: A first-principle relationship between molecular diffusion and viscosity. *AIP Advances*, 10(3). <https://doi.org/10.1063/1.5131234>
- Gmehling, J., Li, J., & Schiller, M. (1993). A modified UNIFAC model. 2. Present parameter matrix and results for different thermodynamic properties. *Industrial & Engineering Chemistry Research*, 32(1), 178–193. <https://doi.org/10.1021/ie00013a024>
- Hawkes, S. J. (1995). Raoult's law is a deception. *Journal of Chemical Education*, 72(3), 204. <https://doi.org/10.1021/ed072p204>
- Hsieh, C.-M., Sandler, S. I., & Lin, S.-T. (2010). Improvements of COSMO-SAC for vapor–liquid and liquid–liquid equilibrium predictions. *Fluid Phase Equilibria*, 297(1), 90–97. <https://doi.org/10.1016/j.fluid.2010.06.011>
- Hung, Y.-C., Su, S.-W., Yan, J.-W., & Hong, G.-B. (2024). Vapor-liquid equilibrium for binary systems containing n-alkanes and cycloalkanes. *Fluid Phase Equilibria*, 578, 114004. <https://doi.org/10.1016/j.fluid.2023.114004>



- IATA. (2025). Our Commitment to Fly Net Zero by 2050. International Air Transport Association. https://www.iata.org/en/programs/sustainability/flynetzero/?utm_source=chatgpt.com
- Kroenlein, K., Muzny, C., Kazakov, A., Diky, V., Chirico, R., & Magee, J. (2012). *NIST Standard Reference 203, TRC Web Thermo Tables (WTT)*. National Institute of Standards and Technology, Gaithersburg, Maryland.
- Kunz, O., & Wagner, W. (2012). The GERG-2008 Wide-Range Equation of State for Natural Gases and Other Mixtures: An Expansion of GERG-2004. *Journal of Chemical & Engineering Data*, 57(11), 3032–3091. <https://doi.org/10.1021/jc300655b>
- Lemmon, E. W., Bell, I. H., Huber, M. L., & McLinden, M. O. (2013). *NIST Standard Reference Database 23: Reference Fluid Thermodynamic and Transport Properties-REFPROP, Version 8.0, Natl Std. Ref. Data Series* (NIST NSRDS). National Institute of Standards and Technology, Gaithersburg, Maryland.
- Linstrom, P. J., & Mallard, W. G. (2001). The NIST Chemistry WebBook: A Chemical Data Resource on the Internet. *Journal of Chemical & Engineering Data*, 46(5), 1059–1063. <https://doi.org/10.1021/jc000236i>
- Lísal, M., Smith, W. R., & Nezbeda, I. (1999). Accurate Computer Simulation of Phase Equilibrium for Complex Fluid Mixtures. Application to Binaries Involving Isobutene, Methanol, Methyl tert-Butyl Ether, and n-Butane. *Journal of Physical Chemistry B*, 103(47), 10496–10505. <https://doi.org/10.1021/jp991188f>
- Lundberg, G. W. (1964). Thermodynamics of Solutions XI. Heats of Mixing of Hydrocarbons. *Lundberg, G. (1964). Thermodynamics of Solutions XI. Heats of Mixing of Hydrocarbons. Journal of Chemical & Engineering Data*, 9, 193–198. <https://doi.org/10.1021/JE60021A013>
- Mendes, G., Aleme, H. G., & Barbeira, P. J. S. (2017). Reid vapor pressure prediction of automotive gasoline using distillation curves and multivariate calibration. *Fuel*, 187, 167–172. <https://doi.org/10.1016/j.fuel.2016.09.046>
- Miller, J. H., Tiftt, S. M., Wiatrowski, M. R., Thathiana Benavides, P., Huq, N. A., Christensen, E. D., Alleman, T., Hays, C., Luecke, J., Kneucker, C. M., Haugen, S. J., Sánchez i Nogué, V., Karp, E. M., Hawkins, T. R., Singh, A., & Vardon, D. R. (2022). Screening and Evaluation of Biomass Upgrading Strategies for Sustainable Transportation Fuel Production with Biomass-Derived Volatile Fatty Acids. *iScience*, 25(11). <https://doi.org/10.1016/j.isci.2022.105384>
- Ministry of Defence. (2025). Defence Standard 91-091: Turbine Fuel, Kerosene Type, Jet A-1; NATO Code: F-35; Joint Service Designation: AVTUR (Issue 18). United Kingdom. <https://www.jig.org/documents/defstan-91-091-issue-18/>
- Mondragon, F., & Ouchi, K. (1984). New method for obtaining the distillation curves of petroleum products and coal-derived liquids using a small amount of sample. *Fuel*, 63(1), 61–65. [https://doi.org/10.1016/0016-2361\(84\)90256-4](https://doi.org/10.1016/0016-2361(84)90256-4)
- Opacich, K. C., Peiffer, E., & Heyne, J. S. (2019). Analyzing the Relative Impact of Spray and Volatile Fuel Properties on Gas Turbine Combustor Ignition in Multiple Rig Geometries (AIAA 2019-1434). *AIAA Scitech 2019 Forum*. <https://doi.org/10.2514/6.2019-1434>
- Poling, B. E., Prausnitz, J. M., & O'Connell, J. P. (2001). *Properties of Gases and Liquids* (5th ed). Graw-Hill Education: Columbus, Ohio.
- Rauch, B. (2017). Systematic Accuracy Assessment for Alternative Aviation Fuel Evaporation Models [Doctoral Thesis, Universität Stuttgart]. Stuttgart, Germany.
- State Bureau of Technical Supervision. (1997). GB/T 6539-1997: Standard test methods for electrical conductivity of aviation and distillate fuels. National Standard of the People's Republic of China. <https://www.chinesestandard.net/PDF/English.aspx/GBT6539-1997>
- Striebich, R. C., Shafer, L. M., Adams, R. K., West, Z. J., DeWitt, M. J., & Zabarnick, S. (2014). Hydrocarbon group-type analysis of petroleum-derived and synthetic fuels using two-dimensional gas chromatography. *Energy Fuels*, 28, 5696–5706. <https://doi.org/10.1021/ef500813x>
- Trinklein, T. J., Prebihalo, S. E., Warren, C. G., Ochoa, G. S., & Synovec, R. E. (2020). Discovery-based analysis and quantification for comprehensive three-dimensional gas chromatography flame ionization detection data. *Journal of Chromatography A*, 1623. <https://doi.org/10.1016/j.chroma.2020.461190>
- Trouton, F. (1884). IV. On molecular latent heat. *The London, Edinburgh, and Dublin Philosophical Magazine and Journal of Science*, 18(110), 54–57. <https://doi.org/10.1080/14786448408627563>
- Wagner, W. (1973). New vapour pressure measurements for argon and nitrogen and a new method for establishing rational vapour pressure equations. *Cryogenics*, 13, 470–482. [https://doi.org/10.1016/0011-2275\(73\)90003-9](https://doi.org/10.1016/0011-2275(73)90003-9)
- Wilson, G. M. (1964). Vapor-Liquid Equilibrium. XI. A New Expression for the Excess Free Energy of Mixing. *Journal of the American Chemical Society*, 86(2), 127–130. <https://doi.org/10.1021/ja01056a002>
- Yang, Z., Boehm, R. C., Bell, D. C., & Heyne, J. S. (2023). Towards sustainable aviation fuel distillation optimization. *Fuel*, 353. <https://doi.org/10.1016/j.fuel.2023.129136>
- Yang, Z., Kosir, S., Stachler, R., Shafer, L., Anderson, C., & Heyne, J. S. (2021). A GC × GC Tier α combustor operability prescreening method for sustainable aviation fuel candidates. *Fuel*, 292. <https://doi.org/10.1016/j.fuel.2021.120345>



Task 2 – Vapor Pressure Measurement for Sustainable Aviation Fuel

Washington State University

Objectives

The objectives of this task are intended to improve the current understanding of vapor pressure of approved SAF pathways and to develop and/or validate blending rules for vapor pressure.

Research Approach

There are several technical issues related to fuel vapor pressure. One key issue is the evaporation rate at temperatures below the boiling point. This rate is influenced by factors such as mass transfer rate, vapor pressure, and surface area. The evaporation rate directly affects droplet evaporation and the dry-out rate of purged staged circuits. Another concern is the pressure inside closed vessels, which can lead to "burping" and coking issues. These arise in systems such as the fuel metering unit and the fuel nozzle valve inlets during shutdown. Vapor pressure is also critical in simulated distillation modeling. During evaporation or vaporization, the composition of both liquid and gas-phase fuel evolves. This causes variations in chemical properties, such as derived cetane number (DCN) or threshold soot index (TSI), in the vapor phase. Furthermore, as the composition of lighter and heavier fractions changes, the vapor pressure and, consequently, the evaporation rate of the liquid phase will fluctuate throughout the process.

The vapor pressure measurements were performed using a PAC® Herzog HVP 972 instrument in accordance with ASTM D6378 (ASTM International, 2022). However, the instrument is currently out of order and unable to measure vapor pressure. Some experimental work has been conducted at Trinity College Dublin, and we are actively exploring the purchase of a replacement vapor pressure analyzer.

Milestone

Measured vapor pressure for two approved SAFs and two SAF candidates.

Major Accomplishments

Published new vapor pressure prediction model.

Publications

Boehm, R., Parker, R., Yang, Z., Dooley, S., & Heyne, J. (2025). Blend Prediction Model for Vapor Pressure of Jet Fuel Range Hydrocarbons. *Sustainability*, 17(21), 9612. <https://doi.org/10.3390/su17219612>

Outreach Efforts

None.

Awards

Joshua Heyne – 2024 Energy and Fuels Rising Starts

Student Involvement

Washington State University PhD student, Zhibin (Harrison) Yang, leads this effort. Joshua Ledezma, an undergraduate student at Washington State University, participated in this effort.

Plans for Next Period

- Continue measurements for vapor pressure of neat molecules, blends, and SAFs.
- Looking into a new vapor pressure machine for low temperature vapor pressure measurements.

Reference

ASTM International. (2022). ASTM D6378-22: Standard Test Method for Determination of Vapor Pressure (VPX) of Petroleum Products, Hydrocarbons, and Hydrocarbon-Oxygenate Mixtures (Triple Expansion Method). <https://doi.org/10.1520/D6378-22>